First-principles study of structural stabilities, and electronic and optical properties of CaF_2 under high pressure

Xiang Wu,[1] Shan Qin,[2] and Ziyu Wu[1,*]
[1]*Beijing Synchrotron Radiation Facility, Institute of High Energy Physics, Chinese Academy of Sciences, Beijing 100049, China*
[2]*Department of Geology, Peking University, Beijing 100871, China*
(Received 26 November 2005; revised manuscript received 21 February 2006; published 7 April 2006)

An investigation into the structural stabilities and the electronic and optical properties of CaF_2 under high pressure was conducted using first-principles calculations based on density functional theory. Our results demonstrate that the sequence of the pressure-induced phase transition of CaF_2 is the fluorite structure ($Fm3m$), the $PbCl_2$-type structure ($Pnma$), and the Ni_2In-type structure ($P6_3/mmc$). At these phase transformations, the coordination number of Ca^{2+} increases from eight to nine and then to eleven. The mechanisms of the structure change were revealed from the $PbCl_2$-type phase to the Ni_2In-type phase. The energy band gap increases with pressure in the $Fm3m$ and the $Pnma$ phases, but decreases in the $P6_3/mmc$ phase. The band gap pressure coefficients were obtained using a linear pressure-dependent fit function. In addition, the energy band overlap metallization does not occur up to 218 GPa. The static dielectric constants ε_0 vs pressure are also discussed.

DOI: 10.1103/PhysRevB.73.134103 PACS number(s): 61.50.Ks, 62.50+p, 71.15.Mb, 81.40.Tv

I. INTRODUCTION

CaF_2, a well-known face-centered-cubic ionic crystal, is commonly designated as a lens material for photolithography at wavelengths in the deep ultraviolet region, due to its excellent transmission properties without absorption bands over a wide wavelength range from UV to IR. These optical properties are related to its structural and electronic properties, such as a very large band gap.[1–5] In addition, CaF_2 is proposed have an excellent internal pressure calibration in moderate high-pressure and (or) high-temperature x-ray diffraction experiments,[6–10] e.g., the achievable precision of volume determination of quartz single crystals to 9.0 GPa allows for pressure precision as high as 0.05–0.1%.[9] Therefore structural stabilities, and electronic and optical properties of CaF_2 are of much theoretical and experimental interest.[1–19]

Pressure-induced phase transformations of CaF_2 have been reported by many research groups.[11–13,15–19] In the first report of CaF_2 as a function of pressure in 1966, Seifert showed that it undergoes a pressure-induced phase transition from the fluorite structure ($Fm3m$) to an orthorhombic $PbCl_2$-type structure ($Pnma$) in the pressure range 8–10 GPa,[11] which has been confirmed by other groups using various methods, such as x-ray diffraction, Raman spectra and theoretical calculations.[12–14,16–19] Recently the initial stages of phase transformations in CaF_2 have been investigated in detail by means of the strain gauge technique in an ideal hydrostatic pressure at room temperature, which indicates that the phase transition pressure is 8.01 ± 0.01 GPa.[18] The high-pressure phase ($Pnma$) has been shown to still be stable up to 49 GPa at room temperature by x-ray diffraction and Raman spectra.[13,16] The phase transition occurs at room temperature but is reversible under these conditions, with the $Pnma$ phase reverting to the $Fm3m$ during decompression. However, single crystals of CaF_2 in the $PbCl_2$-type structure, grown at 8.6 GPa and 1100 K in a molten $Ca(0H)_2$ flux, are stable at ambient conditions.[20] Moreover, the post-$PbCl_2$ structure of divalent metal halides is also of considerable current interest. There are three candidate phases for the post-$PbCl_2$: the Co_2Si structure ($Pnam$, CN=10),[21], the distorted Co_2Si structure ($P2_1/a$, CN=10) for ACl_2 (A=Pb, Ba, and Sn)[22] and the Ni_2In structure ($P6_3/mmc$, CN=10) for AF_2 (A=Pb and Ba),[23–26], respectively. The choice of the high-pressure structure is governed by the cation-anion radius ratio r_c/r_a.[21] The corresponding value for CaF_2 is closer to those of BaF_2 and PbF_2. In addition, Ca and Ba are II A elements. Therefore, we may extrapolate that the high-pressure behavior of CaF_2 is similar to those of BaF_2 and PbF_2, namely with the Ni_2In structure at extreme pressure. However, no reports about the post-$PbCl_2$ phase of CaF_2 have been published up to now.

Experimentally, the indirect gap of CaF_2 was estimated to be 11.8 eV at ambient condition[1] and the dielectric tensors (ε_1 and ε_2) were measured directly using a vacuum ultraviolet spectroscopic ellipsometer with light from a synchrotron source.[2] Different theoretical calculations of CaF_2 bulk electronic structure and optical properties have been compared and discussed extensively.[3–5,17,19,27,28] However, only a few articles described the influence of pressure on the electronic and optical properties of CaF_2.[17,19] More recently, theoretical calculations have shown that the band gap of CaF_2 increases with increasing pressures,[17,19] and it becomes a direct gap from the $Fm3m$ phase to the $Pnma$ phase.[17] On further compression, the gap closes and band overlap metallization occurs around 210 GPa.[17] The increase of the static dielectric constants ε_0 of the fluorite phase is practically linear with pressure.[19]

From the above it is clear that pressure is certainly a critical parameter for the structural stabilities, and electronic and optical properties. The aim of this present work therefore is to explore the influence of pressure on the electronic and optical properties of CaF_2 in detail by electronic structure calculations, which have been proven to be successful in

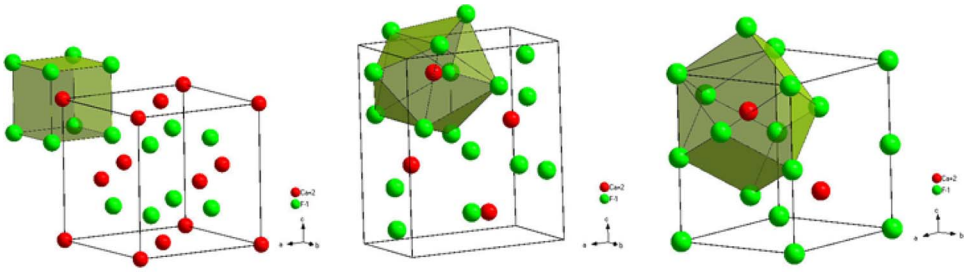

FIG. 1. (Color online) The crystal structures of CaF_2 with space groups $Fm3m$ (a), $Pnma$ (b), and $P6_3/mmc$ (c).

studying the phase transition in our previous work.[29,30] First, we must confirm the high-pressure phases ($Pnma$ and $P6_3/mmc$) and obtain the equation of state, then provide detailed information on the electronic and optical properties, and finally discuss the effect of pressure on the structural stabilities, and electronic and optical properties of CaF_2.

II. METHOD OF CALCULATIONS

According to the literature mentioned above, we designed three possible candidate phases of CaF_2, $Fm3m$, $Pnma$, and $P6_3/mmc$, respectively. The experimental unit cell parameters were used as the initial models for these phases. The atomic positions for the $Fm3m$ phase are Ca (0, 0, 0) and F (1/4, 1/4, 1/4) and the lattice constant a is 5.4630 Å.[31] The Ca and F ions of the $PbCl_2$-type phase occupy the positions (0.2539, 1/4, 0.1094), (0.8595, 1/4, 0.0731), and (0.4780, 1/4, 0.8344), respectively; the lattice constants are a =6.018 Å, b=3.614 Å, and c=7.023 Å.[20] Those of the Ni_2In-type phase are Ca (1/3, 2/3, 1/4), F1 (0, 0, 0), F2 (1/3, 2/3, 1/4), and a=4.253 Å, c=5.516 Å, γ=120°.[23] Fig-

TABLE I. Lattice constants at zero pressure and bulk modulii of three candidate phases for CaF_2.

	Fm3m		*Pnma*		*P6₃/mmc*
	Theoretical	Experimental	Theoretical	Experimental	Theoretical
Lattice constants (Å)	a_0=5.5252[G]	a_0=5.466[c]	a_0=6.0274[G]	a_0=5.63±0.11[c]	a_0=3.8851[G]
	5.3252[L]	5.4630[i]	b_0=3.6682	b_0=3.49±0.03	c_0=5.9267
	5.52[a]		c_0=7.0413	c_0=7.15±0.07	
	5.563[d]				a_0=3.7869[L]
	5.444[d]		a_0=5.7775[L]	a_0=6.018[h]	c_0=5.4135
	5.3378[f]		b_0=3.4830	b_0=3.614	
	5.515[g]		c_0=6.8491	c_0=7.023	
			a_0=6.069[d]		
			b_0=3.643		
			c_0=7.109		
			a_0=5.5029[f]		
			b_0=3.4111		
			c_0=6.9888		
Bulk modulus (GPa)	77[G], 103[L]	81.0±1.2[b]	75[G], 105[L]		62[G]
	91[a]	87±5[c]	86[d]		91[L]
	84.7, 82.7[d]	82.0±0.7[e]	154[f]		
	103[f]	81.1[j]			
	82.14[g]	84.7[k]			

G is the result using GGA in this work; L is the result using LDA in this work.
[a]Reference 5;
[b]Reference 7;
[c]Reference 13;
[d]Reference 14;
[e]Reference 16;
[f]Reference 17;
[g]Reference 19;
[h]Reference 20;
[i]Reference 29;
[j]Reference 37;
[k]Reference 38.

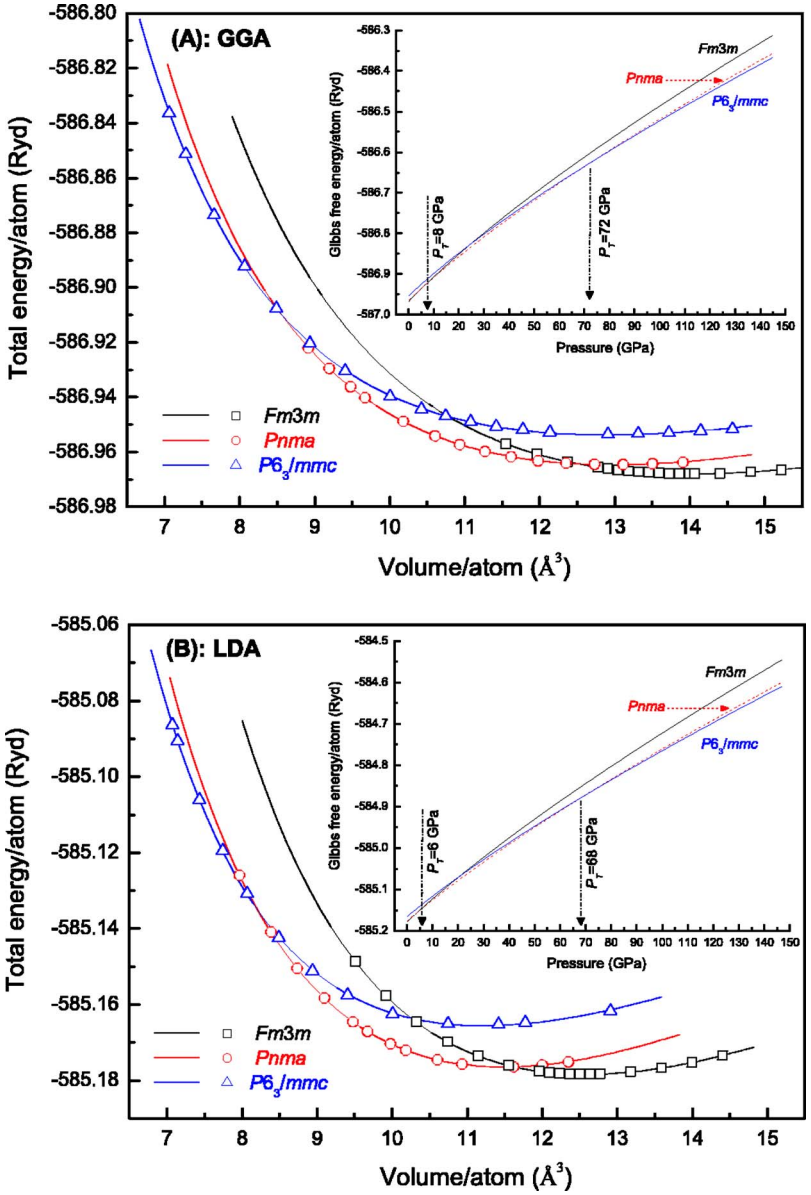

FIG. 2. (Color online) Calculation of the total energy vs volume for the $Fm3m$ phase, the $Pnma$ phase and the $P6_3/mmc$ phase of CaF_2. The inset: calculated Gibbs free energy vs pressure for all phases. (A) GGA; (B) LDA.

ure 1 represents the schematic crystal structures of three candidate phases of CaF_2.

The first-principles calculations performed in this paper are based on the density functional theory (DFT). The total energies were calculated within the full potential linearized augmented plane wave (FPLAPW)+local orbitals (lo) method, implemented in WIEN2K code.[32] The effects of the approximation to the exchange-correlation energy were treated by the generalized gradient approximation (GGA)[33] and the local density approximation (LDA).[34] It is well known that LDA and GGA to DFT systematically underestimate the band gap in semiconductors and insulators (an error of a factor 2). The Engel-Vosko approximation (EVA)[35] seems to lead to better band gaps rather than LDA and GGA, but it cannot give reliable total energies. Therefore, EVA was considered in our calculations of the electronic and optical properties based on the optimized structure models by GGA. In order to increase the reliability and a reasonable comparison, we used the same radius of the muffin-tin sphere for the same kind of atom in all of the calculations. The muffin-tin radii of Ca and F were chosen at 1.6 and 1.7 a.u., respectively. In the LAPW calculations, we set the energy threshold between the core and valence states at −6.0 Ry. For the number of plane waves, the criterion used was the muffin-tin radius multiplied by K_{max} (for the plane waves) yielding a value of 7.0. 2000 k points were specified in the whole Brillouin zone (BZ), which generated 47, 140, and 76 k meshes for the $Fm3m$, $Pnma$, and $P6_3/mmc$, respectively. For each crystalline phase, we calculated the minimum total energy of the unit cell for a number of different volumes. Due to symmetry without atomic positions to relax in the $Fm3m$ and $P6_3/mmc$ cases, we only specified the convergence criterion (the different charge <0.0001) in the self-consistency cycle. In the case of the $Pnma$ phase, we optimized the c/a ratio and the b/a ratio for each volume and relaxed all of the independent internal atomic coordinates until forces on every atom were below a tolerance value taken as 1 mRy/bohr.

TABLE II. Phase transition pressures of CaF_2 and the volume collapses correspondingly.

	Fm3m-to-*Pnma*		*Pnma*-to-*P6$_3$/mmc*
	Theoretical	Experimental	Theoretical
Transition pressure (GPa)	8[G]	8-10[l,m]	72[G]
	6[L]	7.75-9.5[c]	68[L]
	4, 7[d]	8.7-9.5[e]	
	9.1[f]	8.01[n]	
Volume collapses	7.1%[G]	8.1%[l]	2.4%[G]
	8.2%[L]	10%[m]	2.5%[L]
	10%[d]	11%[c]	
	7%[f]	8.3[n]	
		6.3%[n]	

G is the result using GGA in this work; L is the result using LDA in this work
[c]Reference 13;
[d]Reference 14;
[e]Reference 16;
[f]Reference 17;
[h]Reference 20;
[l]Reference 11;
[m]Reference 12;
[n]Reference 18.

Once the minimum total energies of every phase were obtained at different volumes, they were fitted to the Murnaghan equation of state[36] as below:

$$E(V) = E_0 - \frac{B_0 V_0}{B_0' - 1} + \frac{B_0 V}{B_0'}\left[\frac{(V_0/V)^{B_0'}}{B_0' - 1} + 1\right]. \quad (1)$$

Where B_0 and B_0' are the bulk modulus and its derivative, respectively, E_0 is the ground-state total energy and V_0 is the equilibrium volume. On the other hand, the relevant thermodynamic potential is the Gibbs free energy (G) and the stable structure is the one with the lowest G. In this study the temperature is limited to $T=0$ K, so that G is

$$G(P) = E_0 + \frac{B_0 V_0}{B_0' - 1}\left[\left(1 + \frac{B_0'}{B_0}P\right)^{(B_0'-1)/(B_0')} - 1\right]. \quad (2)$$

If a first-order transition between two phases occurs, in both phases G will be equal at the transition pressure P_T. Alternatively, the transition pressure may be obtained as the negative slope of the common tangent between the two $E_{tot}(V)$ curves.

The frequency dependent complex dielectric function $\varepsilon(\omega)=\varepsilon_1(\omega)+i\varepsilon_2(\omega)$ is known to describe the optical response of the medium. For dielectric tensor calculations, the BZ integration was performed using the tetrahedron method with 1200 k points without broadening in all phases. The imaginary part $\varepsilon_2(\omega)$ was obtained from the electronic structure calculation, using the joint density of states and the optical matrix elements. The real part $\varepsilon_1(\omega)$ was derived from

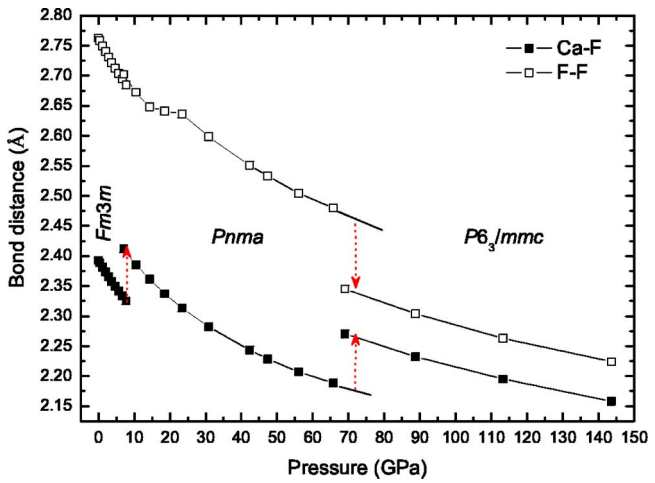

FIG. 3. (Color online) The mean Ca-F distance and the mean F-F distance calculated from the GGA results vs pressure.

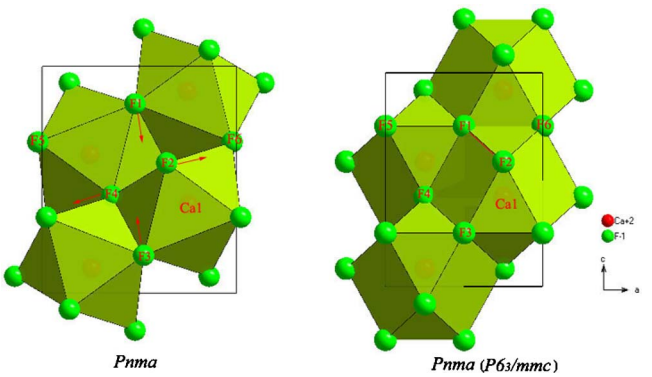

FIG. 4. (Color online) Projection along the b axis of two orthorhombic phases (the $PbCl_2$-type structure and the Ni_2In-type structure).

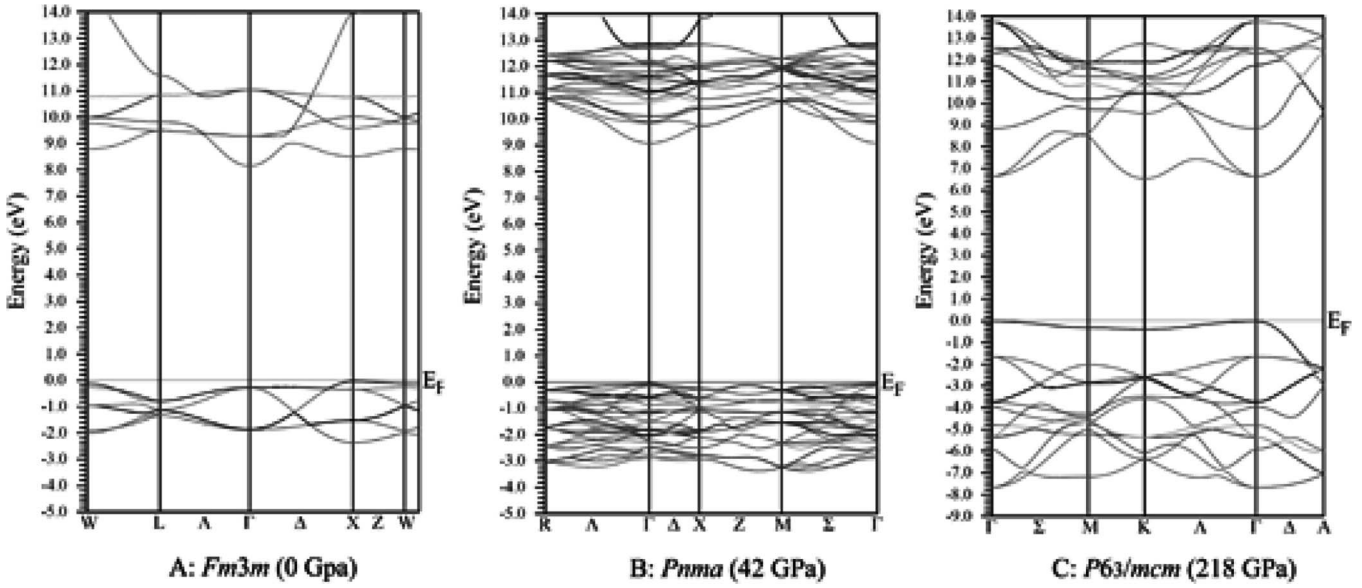

FIG. 5. Energy band structures of CaF_2 at different pressures calculated by the EVA. (A) The fluorite-type phase at zero pressure, the indirect band gap $X \rightarrow \Gamma$; (B) the $PbCl_2$-type phase at 42 GPa, the direct band gap $\Gamma \rightarrow \Gamma$; (C) the Ni_2In-type phase at 218 GPa, the indirect band gap $\Gamma \rightarrow K$.

$\varepsilon_2(\omega)$ by using the Kramers-Krönig relationship. In order to obtain the isotropic static dielectric constants ε_0, or $\varepsilon_1(0)$, the components of the matrix trace were averaged by a sum over states, namely, $\varepsilon_{iso}(0)=[\varepsilon_{xx}(0)+\varepsilon_{yy}(0)+\varepsilon_{zz}(0)]/3$ for the *Pnma* phase and $\varepsilon_{iso}(0)=[2\varepsilon_{xx}(0)+\varepsilon_{zz}(0)]/3$ for the $P6_3/mmc$ phase.

III. RESULTS AND DISCUSSION

A. Structural stabilities

The theoretical ground-state parameters (lattice parameters and B_0) of CaF_2 are obtained and listed in Table I, which also includes the available experimental and theoretical data for comparison. It is clear that our theoretical values agree very well with the experimental data,[5,14,17,19] as well as with other calculations.[13,20,29] The LDA generally underestimates the lattice constants while the GGA overestimates them when compared with experiments. The bulk moduli differ by up to 30 GPa between the LDA and the GGA, as seen Table I, but the GGA in the present calculations yield values closer to the experiments. The bulk moduli only present a slight change, in our calculations, from the *Fm*3*m* phase to the *Pnma* phase, which is also reported in Ref. 14 and is similar to that of PbF_2.[26] However, the B_0 of the CaF_2 *Pnma* phase is 154 GPa bigger than that of the *Fm*3*m* phase in Ref. 17 with the tight binding linear muffin-tin orbital (TB-LMTO) method. The possible reasons for this discrepancy are that the LMTO method is not accurate in the case of axial ratio minimization and (or) five empty spheres were added in the *Pnma* phase in their calculations. The B_0 of $P6_3/mmc$ presents a significant decrease, which indicates CaF_2 will become softer at extreme high pressure.

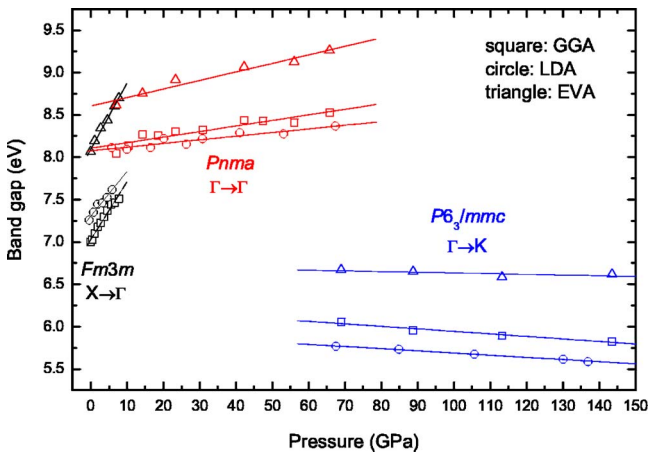

FIG. 6. (Color online) The energy band gap of CaF_2 vs pressure.

The total energy, calculated as a function of the volume for three phases, is compared in Fig. 2. The solid lines are the fit of the computed data using the Murnaghan equation of state [Eq. (1)]. In Fig. 2, we observed the following sequence of phase transition in CaF_2: $Fm3m \rightarrow Pnma \rightarrow P6_3/mmc$. The insets of Fig. 2 illustrate curves of the Gibbs free energies calculated as a function of pressure according to Eq. (2). The first transition (*Fm*3*m* to *Pnma*) takes place at 8 GPa and the second (*Pnma* to $P6_3/mmc$) at 72 GPa in the GGA, and 6 GPa and 68 GPa correspondingly in the LDA. The

TABLE III. The pressure coefficient for the energy band gap of CaF_2 in three candidate phases (eV/GPa).

	GGA	LDA	EVA
*Fm*3*m*	0.0684	0.0528	0.0785
Pnma	0.0066	0.0043	0.0101
$P6_3/mmc$	−0.0030	−0.0026	−0.0007

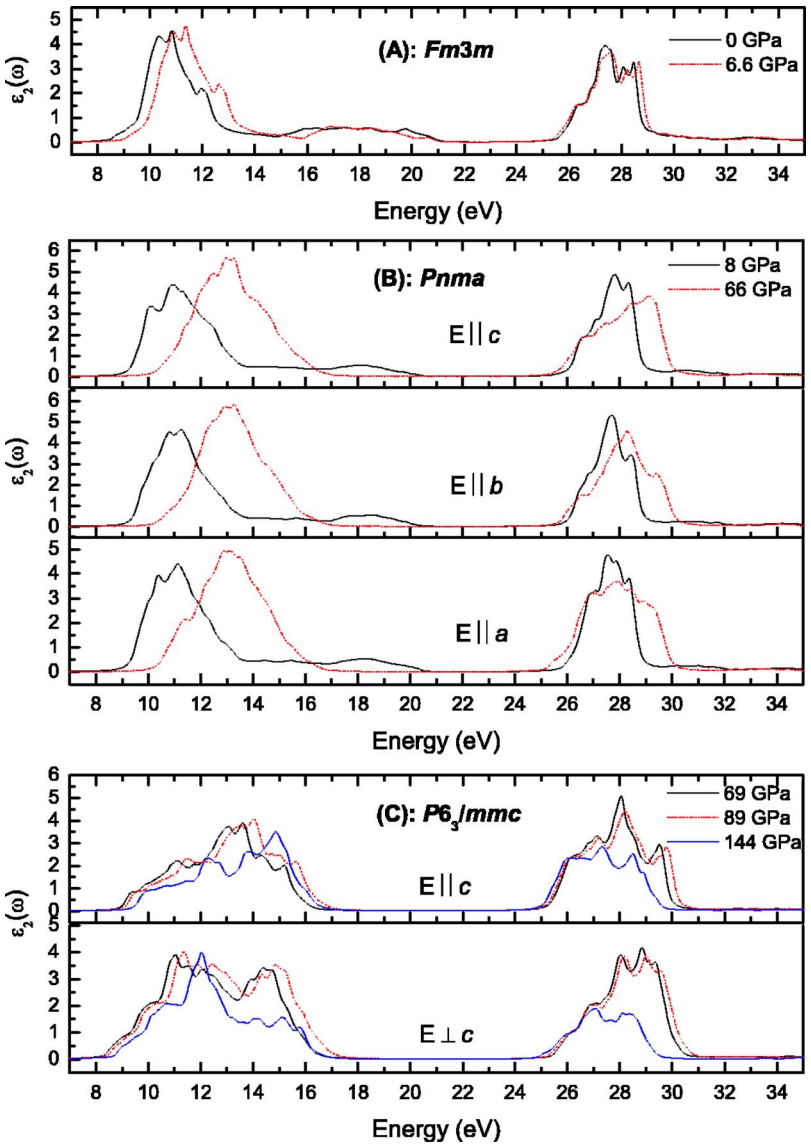

FIG. 7. (Color online) The imaginary part of the dielectric function of CaF_2 vs photon energy at differential pressure calculated by FPLAPW with EVA; (A) the fluorite-type phase, an isotropic system; (B) the $PbCl_2$-type phase, an anisotropic system. The E$\|a$, E$\|b$, and E$\|c$ light polarizations are calculated and shown; (C), the Ni_2In-type phase, the E$\|c$ and E$\perp c$ are also shown.

volume collapses have been calculated at transition pressures. Table II summarizes the transition pressures and the volume collapse of CaF_2, also inconsistant with available experimental data.

The coordination of Ca^{2+} of eightfold, ninefold and eleven-fold for the *Fm*3*m*, the *Pnma*, and the $P6_3/mmc$ are displayed in Fig. 1, respectively. It is well known that the ionic radius increases as the coordination number increases, e.g., 1.12 Å for Ca^{2+}(VIII), 1.18 Å for Ca^{2+}(IX), 1.23 Å, for Ca^{2+}(X), and 1.34 Å for Ca^{2+}(XII).[39] The mean Ca-*F* distance, calculated from the average of the distances between the Ca^{2+} and all its coordinated F^{1-} using the results of GGA, decreases in each phase on compression, but it increases suddenly at the two phase transition pressures (8 and 72 GPa), as shown in Fig. 3. At the boundary of phase transition (the *Fm*3*m* to the *Pnma*), the increase of the Ca-*F* distance is 0.08 Å and in good agreement with the increases deduced from the ionic radii of Ca^{2+} between eightfold and ninefold given above. At the other phase transition the increase of the mean Ca-*F* distance is 0.10 Å, which extrapolates the radius of Ca^{2+}(XI) as 1.28 Å. Figure 3 also shows that the nearest-neighbor bond distances of *F*-*F* decrease with increasing pressure. Especially at 72 GPa, the decrease of the *F*-*F* distance is larger, which is attributed to the environment change of the first cluster of F^{1-}. There are ten ions ($4\ Ca^{2+}+6F^{1-}$) around one F^{1-} in the *Pnma*, fourteen ions ($6\ Ca^{2+}+8\ F^{1-}$) in the $P6_3/mmc$. The radius of F^{1-} may be considered as a constant, thus the *F*-*F* distance must rapidly decrease in order to offset the increase of the Ca-*F* distance at the phase transition pressure.

In order to understand of the mechanisms of the structure change from the $PbCl_2$-type phase to the Ni_2In-type phase, we describe the hexagonal Ni_2In structure as an orthorhombic structure, also of the space group *Pnma*, where $a_0=c_h$, $b_0=a_h$, $c_0=3^{1/2}a_h$, and the atomic positions of Ca are (1/4, 1/4, 1/12), and of *F* are (1/4, 1/4, 5/12) and (0,3/4,1/4).[23] Projection along the *b* axis of these two orthorhombic structures is shown in Fig. 4. According to the optimized atomic positions of the *Pnma* phase at various pressures, the paths of some fluorine ions shift are labeled, as the arrows indicate in Fig. 4. The $<F5$-$F1$-$F6$ increase with pressure increasing in the $PbCl_2$ structure and become 180° in the Ni_2In struc-

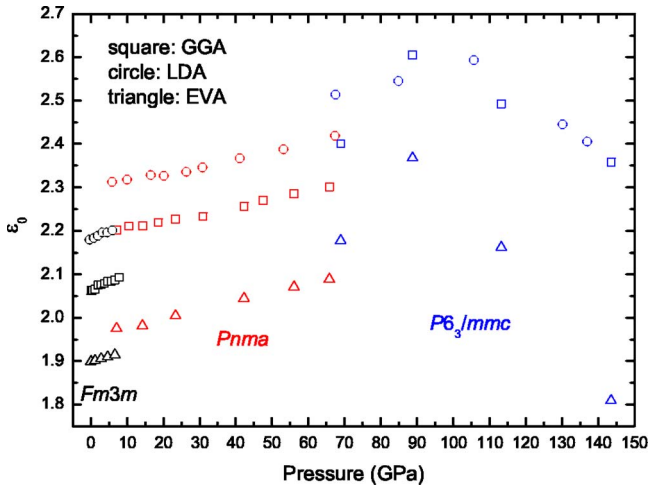

FIG. 8. (Color online) Pressure dependence of the static dielectric constants ε_0.

ture. The $F1$ ion shifts to the coordination polyhedron of Ca1 on compression and becomes a coordination of Ca1 in the $P6_3/mmc$. The other F^{1-} ion in the back is of the same behavior, thus the coordination number of Ca^{2+} adds two and becomes finally eleven at the phase transition from the *Pnma* to the $P6_3/mmc$. In other words, this phase transition involves a rotation of the coordination polyhedrons of Ca along the *b* axis.

B. Electronic properties

The self-consistent band structures for CaF_2 were obtained at ambient as well as at high pressures. The calculated indirect gap ($X \rightarrow \Gamma$) is 7.27 eV in the LDA or 7.01 eV in the GGA at zero pressure, in agreement with those of references,[3,4,17,19] but it is much smaller than the experimental values (11.8 eV).[1] The reason has been mentioned in Sec. II regarding the calculation method that DFT-LDA (GGA) calculations underestimate the band gap by a factor of typically two. While the band gap calculated using EVA is 8.07 eV at zero GPa, as shown in Fig. 5(a), also less is obtained experimentally.[1] Recently the hybrid B3PW and B3LYP methods have been applied to calculate the band gap, and give better results, i.e., 10.68 eV in B3PW and 10.57 eV in B3LYP.[5] It is well known that the GW calculations give energy band gaps in excellent agreement with experiment, i.e., the band gap is 11.38 eV for CaF_2,[27] nearly close to the experimental value. In a word, the discrepancy is due to the fact that DFT Kohn-Sham states do not take into account the quasiparticle self-energy correctly[40] in our calculations.

Despite the energy band gap underestimated in DFT-LDA (GGA, EVA), its high-pressure behavior can be still compared and discussed in the calculations by using the same exchange-correlation potential. As such we investigated the effect of the pressure on the size of the energy band gap. The gap in both the $Fm3m$ phase and the *Pnma* phase increases with increasing pressure, while there is a sudden decrease at the phase transition from the *Pnma* to the $P6_3/mmc$, as shown in Fig. 6. Figure 5 presents the indirect gap of the $Fm3m$, phase which becomes a direct gap in the *Pnma* phase, and then again an indirect gap in the $P6_3/mmc$. The solid lines in Fig. 6 are least-square fits to the calculated data using a linear pressure-dependent fit function: $E(P)=E(0)+\alpha P$, where the energy E is in eV, the pressure P is in GPa, and α is the band gap pressure coefficient. The α of the $Fm3m$ is positive and larger than that of the *Pnma*, but that of the $P6_3/mmc$ is negative, as seen in Table III. Kanchana *et al.*, reported that the band overlap metallization occurs around 210 GPa in the *Pnma* phase,[17] however, it does not occur at 218 GPa for the $P6_3/mmc$ phase in our calculation, as shown in Fig. 5(c). The inconsistency is due to the factor that the phase transition from the *Pnma* to the $P6_3/mmc$ was not considered in their calculations except for mention in the section of structural properties. The band gap decreases with pressure increasing in the $P6_3/mmc$, but it is very difficult to make it overlap according to the pressure coefficient.

C. Optical properties

The imaginary (absorptive) part of the electronic dielectric function ε_2 was calculated. A selection of ε_2 with EVA and representing three phases at various pressures is shown in Fig. 7. At zero GPa, the major peaks in the range of 6–22 eV are in good agreement with those of Refs. 3 and 19, and inconsistent with the experiment[2] if a shift of 4.2 eV is applied in our calculations; those in the range of 22–34 eV could not be compared as no relative reports were available. All peaks shift toward the high energy with an increase of pressure in the $Fm3m$ and the *Pnma* phases. However, the features from 16 to 21 eV of the *Pnma* phase disappear up to 66 GPa, as shown in Fig. 7(b). In the $P6_3/mmc$ phase, the ε_2 becomes very complicated. First, the peaks also shift to the high energy in the pressure range of 68–90 GPa, but they present abnormal behavior that shifts toward lower energy above 90 GPa. This abnormal variation may be attributed to the stronger pressure dependence in the Σ and Λ directions of the $P6_3/mmc$ phase.

The static dielectric constants ε_0, one of the important optical constants, were also calculated at various pressures. The ε_0 of the $Fm3m$ phase is 2.06 in GGA, 2.17 in LDA, and 1.89 in EVA at zero pressure, which are larger than the extrapolated value of 1.50 for the experiment of Ref. 2. But they are in good agreement with the value of 2.02 in Ref. 3, of 1.89 in Ref. 19, and of 2.04 in Ref. 41. This discrepancy is also due to the shortcoming of DFT ($T=0$ K) as mentioned in the above section. The pressure dependence of ε_0 is illustrated in Fig. 8. As can be seen, the increase of the ε_0 with pressure is linear in the $Fm3m$ phase and the *Pnma* phase. There is an abnormal change of the ε_0 at about 90 GPa in the $P6_3/mmc$, inconsistent with that of the ε_2. The analogous behavior was also observed in the $P6_3/mmc$ phase of BaF_2 under high pressure.[24]

IV. CONCLUSION

In conclusion, *ab initio* calculations have demonstrated that a phase transition of CaF_2 from the fluorite structure ($Fm3m$) to the $PbCl_2$-type structure (*Pnma*) occurs at 8 GPa in GGA or 6 GPa in LDA, in good agreement with other

theoretical and experimental data, and further predicted that the *Pnma* phase will transform into the Ni_2In-type structure at about 70 GPa. At these phase transformations, the coordination number of Ca^{2+} increases from eight to nine and then to eleven. According to the optimized atomic positions of the *Pnma* phase at various pressures, we have revealed the mechanisms of the structure change from the $PbCl_2$-type phase to the Ni_2In-type phase, which involves a rotation of the coordination polyhedrons of Ca along the *b* axis. Pressure not only makes the structural phase transitions of CaF2 occur, but also changes its electronic and optical properties correspondingly. The indirect gap of the *Fm*3*m* phase becomes a direct gap in the *Pnma* phase, and then again becomes an indirect gap in the $P6_3/mmc$. The energy band gap increases with pressure in the *Fm*3*m* and the *Pnma* phases. However, the gap decreases in the $P6_3/mmc$ phase. The pressure coefficients were obtained using a linear pressure-dependent fit function. The energy band overlap metallization does not occur up to 218 GPa. The static dielectric constants ε_0 also increases in the *Fm*3*m* and the *Pnma* phases under compression, but presents an abnormal behavior in the $P6_3/mmc$ phase at about 90 GPa.

ACKNOWLEDGMENTS

Z.Y. Wu acknowledges the financial support of the Outstanding Youth Fund (10125523), the Key Important Nano-Research Project (90206032) of the National Natural Science Foundation of China, and also the Pilot Project of the Knowledge Innovation Program of the Chinese Academy of Sciences (KJCX2-SW-N11). S. Qin thanks the National Natural Sciences Foundation of China for financial support (40272023).

*Corresponding author Electronic address: wuzy@ihep.ac.cn

[1] G. W. Rubloff, Phys. Rev. B **5**, 662 (1971).
[2] J. Barth, R. L. Johnson, M. Cardona, D. Fuchs, and A. M. Bradshaw, Phys. Rev. B **41**, 3291 (1990).
[3] F. Gan, Y. N. Xu, M. Z. Huang, W. Y. Ching, and J. G. Harrison, Phys. Rev. B **45**, 8248 (1992).
[4] M. Verstraete and X. Gonze, Phys. Rev. B **68**, 195123 (2003).
[5] H. Shi, R. I. Eglitis, and G. Borstel, Phys. Rev. B **72**, 045109 (2005).
[6] R. M. Hazen and L. W. Finger, J. Appl. Crystallogr. **14**, 234 (1981).
[7] A. Katrusiak and R. J. Nelmes, J. Appl. Crystallogr. **19**, 73 (1986).
[8] R. J. Angel, J. Phys.: Condens. Matter **5**, L141 (1993).
[9] R. J. Angel, D. R. Allan, R. Miletich, and L. W. Finger, J. Appl. Crystallogr. **30**, 461 (1997).
[10] R. Miletich, D. R. Allan, and W. F. Kuhs, Rev. Mineral. Geochem. **41**, 445 (2001).
[11] K. F. Seifert, Ber. Bunsenges. Phys. Chem. **70**, 1041 (1966).
[12] D. P. Dandekar and J. C. Jamieson, Trans. Am. Crystallogr. Assoc. **5**, 19 (1969).
[13] L. Gerward, J. S. Olsen, S. Steenstrup, S. Åsbrink, and A. Waskowska, J. Appl. Crystallogr. **25**, 578 (1992).
[14] A. M. Pendás, J. M. Recio, M. Flórez, and V. Luaña, Phys. Rev. B **49**, 5858 (1994).
[15] J. H. Burnett, Z. H. Levine, and E. L. Shirley, Phys. Rev. B **64**, 241102(R) (2001).
[16] S. Speziale and T. S. Duffy, Phys. Chem. Miner. **29**, 465 (2002).
[17] V. Kanchana, G. Vaitheeswaran, and M. Rajagopalan, Physica B **328**, 283 (2003).
[18] F. S. El'kin, O. B. Tsiok, L. G. Khvostantsev, and V. V. Brazhkin, J. Exp. Theor. Phys. **100**, 971 (2005).
[19] R. Khenata, B. Daoudi, M. Sahnoun, H. Baltache, M. Rérat, A. H. Reshak, B. Bouhafs, H. Abid, and M. Driz, Eur. Phys. J. B **47**, 63 (2005).
[20] E. Morris, T. Groy, and K. Leinenweber, J. Phys. Chem. Solids **62**, 1117 (2001).
[21] J. Haines, J. M. Leger, and O. Schulte, Phys. Rev. B **57**, 7551 (1998).
[22] J. M. Leger, J. Haines, and A. Atouf, J. Appl. Crystallogr. **28**, 416 (1995); Phys. Rev. B **51**, 3902 (1995); J. Phys. Chem. Solids **57**, 7 (1996).
[23] J. M. Leger, J. Haines, A. Atouf, O. Schulte, and S. Hull, Phys. Rev. B **52**, 13247 (1995).
[24] A. P. Ayala, J. Phys.: Condens. Matter **13**, 11741 (2001).
[25] V. Kanchana, G. Vaitheeswaran, and M. Rajagopalan, J. Alloys Compd. **359**, 66 (2003).
[26] A. Costales, M. A. Blanco, R. Pandey, and J. M. Recio, Phys. Rev. B **61**, 11359 (2000).
[27] E. L. Shirley, Phys. Rev. B **58**, 9579 (1998).
[28] L. X. Benedict and E. L. Shirley, Phys. Rev. B **59**, 5441 (1999).
[29] X. Wu, Z. Y. Wu, L. Guo, C. Liu, J. Liu, and X. D. Li, Solid State Commun. **135**, 780 (2005).
[30] X. Wu, Y. H. Dong, S. Qin, M. I. Abbas, and Z. Y. Wu, Solid State Commun. **136**, 416 (2005).
[31] A. Smakula and J. Kalnajs, Phys. Rev. **99**, 1737 (1955).
[32] P. Blaha, K. Schwarz, WIEN2K, Vienna University of Technology Austria (2002).
[33] J. P. Perdew, K. Burke, M. Ernzerhof, Phys. Rev. Lett. **77**, 3865 (1996).
[34] J. P. Perdew and Y. Wang, Phys. Rev. B **45**, 13244 (1992).
[35] E. Engel and S. H. Vosko, Phys. Rev. B **47**, 13164 (1993).
[36] F. D. Murnaghan, Proc. Natl. Acad. Sci. U.S.A. **50**, 667 (1944).
[37] C. R. A. Catlow, J. D. Commins, F. A. Germano, R. T. Harley, and W. Hayes, J. Phys. C **11**, 3197 (1978).
[38] P. S. Ho and A. L. Ruoff, Phys. Rev. **161**, 864 (1967).
[39] R. D. Shannon, Acta Crystallogr. **32**, 751 (1976).
[40] S. N. Rashkeev and W. R. L. Lambrecht, Phys. Rev. B **63**, 165212 (2001).
[41] W. Y. Chine, F. Gan, and M. Z. Huang, Phys. Rev. B **52**, 1596 (1995).